Light-Controlled Hierarchical Self-Assembly of Polyelectrolytes and Supramolecular Polymers

John B. Matson,[†,‡] Yotam Navon,[§] Ronit Bitton,*,[§] and Samuel I. Stupp[†,‖]

[‖]Departments of Materials Science and Engineering, Chemistry, Medicine, and Biomedical Engineering, Northwestern University, Evanston, Illinois 60208, United States

[†]Simpson Querrey Institute for BioNanotechnology, Northwestern University, Chicago, Illinois 60611, United States

[§]Department of Chemical Engineering and IKI Nanotechnology Institute at Ben Gurion University of the Negev, Beer-Sheva 84105, Israel

Ⓢ *Supporting Information*

ABSTRACT: Dynamic control over supramolecular interactions using various stimuli continues to drive the development of smart materials. We describe here the extension of dynamic self-assembly to a self-assembled hierarchical structure. A peptide amphiphile (PA) was designed with a photocleavable nitrobenzyl ester component such that it would undergo a sphere-to-cylinder transition upon irradiation, as confirmed by cryogenic transmission electron microscopy and small-angle X-ray scattering (SAXS). The photocleavable PA was then tested in the formation of a macroscopic sac made through a complex hierarchical self-assembly process between PA and hyaluronic acid. The micro-structure of the resulting sac has previously been noted to depend dramatically on the geometry of the PA nanostructure. Photolysis of the PA solution during sac formation led to a sac microstructure that displayed characteristics of sacs made with both cylinder-forming PAs and sphere-forming PAs, as measured by scanning electron microscopy and SAXS.
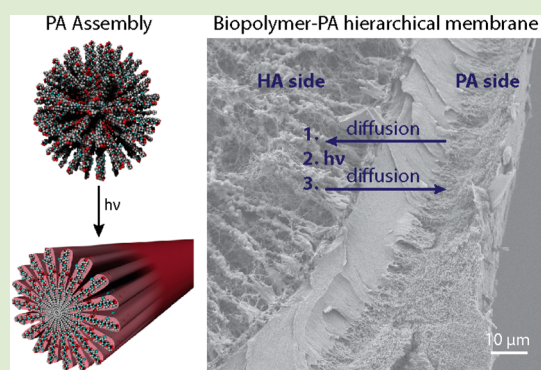
Hierarchical materials, which are structures that exhibit order across several length scales, are prevalent in nature.[1−4] A well-known example is bone, which is made up of nanoscale mineralized collagen fibrils, which aggregate to form micron-sized arrays of fibril bundles, which further assemble to form ordered macroscale bone.[5] Specialized cell types constantly remodel bone and other natural hierarchical materials, providing a biological mechanism for dynamic control over complex structures. The field of synthetic hierarchical materials is relatively new, and attaining *dynamic* control over hierarchical material synthesis remains largely unexplored.[6,7]

The formation of biological hierarchical materials often begins with organization of soft matter components, such as collagen. In 2008 a unique soft hierarchical structure was discovered by bringing into contact aqueous solutions of a polyelectrolyte and self-assembling amphiphiles of opposite charge.[3] Rather than forming an amorphous solid, as is generally expected when oppositely charged components are mixed, an ordered membrane formed. The membrane could also be formed in a spherical shape to generate an enclosed sac. The process for membrane formation was determined to be driven by initial electrostatic complexation of the two components to form a thin dense barrier layer that prevented mixing, followed by osmotic pressure-driven slow diffusion of the large macromolecules through the barrier into the

amphiphile solution. Interactions between the diffusing polymer chains and the fibrous supramolecular structures formed by the amphiphiles led to self-organization of aligned nanofiber bundles, forming the outermost layer of the membrane. Since this initial discovery using peptide amphi-philes and various biopolymers, the approach has been found to be generalizable to a variety of polyelectrolytes and self-assembling small molecules.[8−11] Other peptide-based hierarch-ical assemblies have also been recently reported.[12,13]

Incorporating dynamic tunability into hierarchical materials requires one or more components that can be triggered to undergo changes in structure that affect the final assembled state. External stimuli that can be used for this purpose include pH changes,[14−17] temperature changes,[18−21] photoirradia-tion,[22−28] application of an electric field,[29] and the presence of specific enzymes,[30−34] among others. Of these stimuli, the application of light is generally the most straightforward, as UV irradiation is specific, operationally simple, and can be turned on or off instantaneously.

We sought to extend our previously developed use of light-responsive components in self-assembly[22−24] to hierarchical structures. The demonstration of dynamic control of self-

assembly over multiple length scales would further extend the field of responsive materials. Furthermore, the structural complexity that is possible in synthetic materials could be extended with dynamic systems, leading to better mimics of highly ordered natural materials.

Peptide amphiphiles (PAs) are a broad class of self-assembling peptides that have been used in a variety of biomedical applications.[35−40] In their canonical form, PAs consist of a nonpeptidic hydrophobic segment covalently attached to a peptide sequence.[41,42] Self-assembly of PA molecules in aqueous solution into supramolecular spheres, cylinders, ribbons, tapes, vesicles, and other morphologies has been observed and also investigated using computer simulations.[43−46] Cylinder-forming PAs have found the most utility in biomedical applications due to their ability to form gels upon charge screening.[47] Cylindrical or ribbonlike nanostructures are often the preferred assembly state in PAs that contain a single hydrophobic tail (e.g., palmitic acid), as well as amino acids with high β-sheet propensities adjacent to the hydrophobic tail followed by 2−3 charged residues. Reducing the β-sheet propensity of the amino acids or increasing the number of charged residues tends to favor spherical micelles.[48,49]

In previous studies in the Stupp laboratory, light-responsive PAs were synthesized by covalently binding the 2-nitrobenzyl photocleavable group to the amide nitrogen on the amino acid residue nearest to the hydrophobic tail.[23,24] Cleaving this group was shown to induce a change in the PA morphology from quadruple helices to cylindrical fibers[23] or from spherical micelles to cylindrical nanofibers.[24] Extending these concepts, we recently synthesized a set of PAs containing a photocleavable nitrobenzyl ester group in the peptide backbone, allowing for rapid removal of a bioactive peptide epitope.[22] Here we sought to extend this concept of photocleavable epitopes using the photocleavable unit as a chemical handle for changing the primary sequence of a PA in order to drive a change in its assembled state. PAs assembled into different states (e.g., spherical micelles vs cylindrical nanofibers) form sacs with different morphologies upon mixing with hyaluronic acid (HA);[50] therefore, we anticipated that this strategy would enable dynamic control over sac membrane morphology.

Previous results have shown that the sequence $C_{16}V_3A_3K_3$ (where C_{16} = palmitic acid) assembles into nanofibers of high persistence length, while PAs with a sequence containing a large number of lysine residues (e.g., C_{16}KLAKLAKKLAKLAK) assemble into spherical micelles.[10] Based on these results, we expected that similar highly charged PAs would also form spherical micelles in aqueous solutions. In order to trigger light-driven control from a supramolecular sphere to a cylinder, we incorporated a nitrobenzyl ester into the peptide backbone to generate **PA-1**, which has the sequence $C_{16}V_3A_3K_3$-photo-K_3 (Figure 1; where photo represents the photolabile amino acid).[22] Peptide synthesis was accomplished on a microwave-assisted peptide synthesizer using Fmoc-amino acids and the previously reported photolabile Fmoc-amino acid. Upon photolysis, the PA changes from the sextuply charged $C_{16}V_3A_3K_3$-photo-K_3 sequence to the triply charged $C_{16}V_3A_3K_3G$ sequence (**PA-2**) with loss of a trilysine species. Authentic **PA-2** was also synthesized for comparison.

We assessed the assembly state of PAs **1** and **2** using small-angle X-ray scattering (SAXS) and cryogenic transmission electron microscopy (TEM; Figure 2). As expected, **PA-1** was found to form spherical micelles in aqueous solution by cryo-
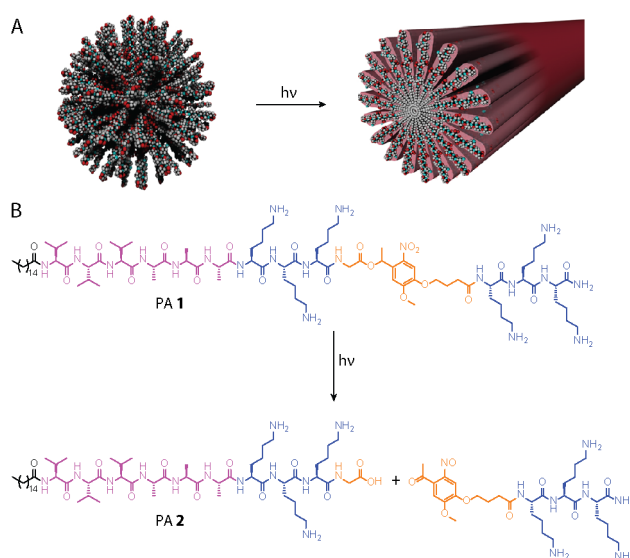

Figure 1. (A) Graphical representation of the sphere to cylinder transition. (B) Chemical structures of **PA-1** and **PA-2**. Color scheme: black = hydrophobic tail; pink = β-sheet sequence; blue = charged sequences; orange = photolabile component.
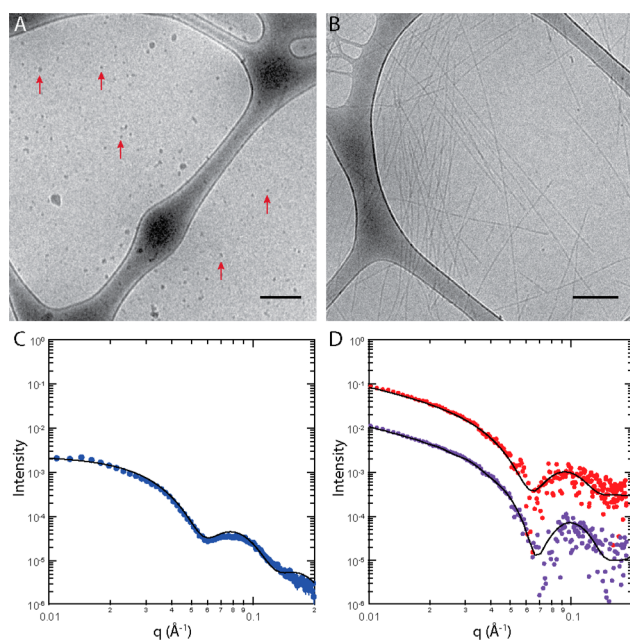

Figure 2. Cryogenic TEM and SAXS traces with fittings (black lines) of **PA-1** (A, C), **UVPA-1** (B and red data points in D), and an authentic sample of **PA-2** (purple data points in D). Red arrows in (A) highlight some of the spherical micelles. SAXS traces in (D) have been offset on the y-axis for clarity. Scale bar = 200 nm.

TEM. These results matched well with SAXS data of **PA-1**, which could be fitted to a polydisperse core−shell sphere model with an average diameter of 12.7 nm (see Supporting Information). Upon photoirradiation with 365 nm light for 20 min, the self-assembly state of the PA changed dramatically, forming long cylindrical nanostructures. Our data are consistent with previously reported results on both authentic **PA-2** and on a similar photocleavable PA that generated **PA-2** upon irradiation.[22] Measurement of the TEM images showed that the nanofibers had a diameter of 9.9 ± 0.6 nm. SAXS data of a sample of photoirradiated **PA-1** (**UVPA-1**) were fitted using a

polydisperse core—shell cylinder model, giving an average nanofiber diameter of 10.3 nm. Fitting of the same model to authentic **PA-2** gave a similar diameter value of 10.2 nm. The morphology change is also evident by the ability of the PA to form a self-supporting gel upon the addition of divalent counterions. Addition of sodium sulfate to **UVPA-1** resulted in gel formation, whereas addition of sodium sulfate to **PA-1** did not.

To investigate how our PA could be incorporated into hierarchical structures, we chose to study the effect of **PA-1** on sacs that can be formed by self-assembling PA nanofibers with oppositely charged polymers, as mentioned above.[3] These complex membranes form when a drop of aqueous HA solution is added to an aqueous solution of positively charged PA. When nanofiber-forming PAs are used, a diffusion barrier forms instantaneously after mixing.[3] Over the next several hours, osmotic pressure drives the migration of the HA polymer chains from the core of the sac through the diffusion barrier to the surface.[51] Once the anionic HA chains are exposed to the PA solution, assembly of cationic PA nanofibers around the HA polymer chains occurs, leading to the formation of aligned fibers perpendicular to the surface of the diffusion barrier. The result is a structure comprised of three zones: an amorphous HA zone in the center of the sac, a dense diffusion barrier zone, and an outermost perpendicular fiber zone. The SEM image in Figure 3B with the three zones labeled is representative of these traditional HA-PA sacs.

The effect of PA nanoscale morphology on the microstructure of hierarchically self-assembled membranes composed of HA and positively charged PAs was recently reported.[10]
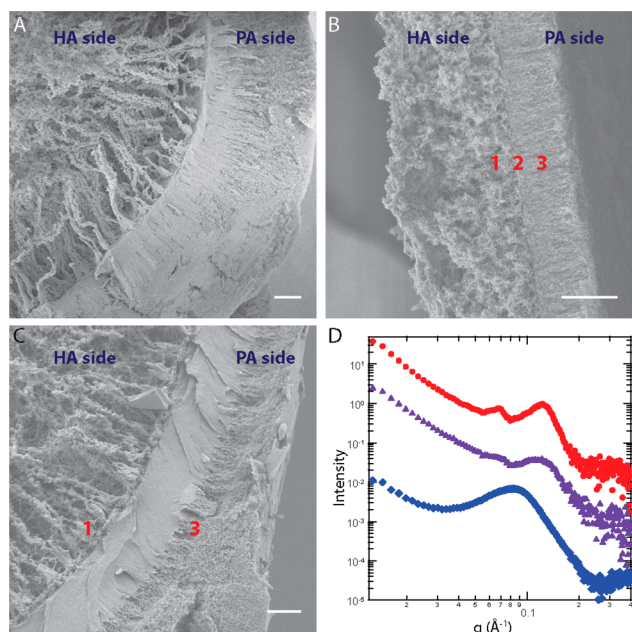

Figure 3. SEM (A—C) and SAXS data (D) of HA-PA sacs made from **PA-1** (A and red data points in D), authentic **PA-2** (B and blue data points in D), and **UVPA-1** (C and purple data points in D). The sac made with **UVPA-1** was allowed to mature in a bath of **PA-1**, after which the sac and bath were irradiated and the sac was allowed to mature further. The red labels 1, 2, and 3 in the SEM micrographs denote the amorphous HA region, the diffusion barrier (only present in B), and the perpendicular fiber region, respectively. The perpendicular fibers in zone 3 are described as such because they are perpendicular to the diffusion barrier (zone 2). Scale bar = 10 μm.

Membranes formed with spherical micelles, rather than cylindrical ones, did not display the thin, dense diffusion barrier and perpendicular fibers typically observed in HA-PA sacs. Instead, these sacs showed an atypical structure with a membrane consisting of a thick cross-section with no obvious contact layer or perpendicular fiber growth. SAXS analysis of these atypical sacs revealed a cubic phase ordering that is likely due to clusters of spherical PA nanostructures surrounded by polyelectrolyte chains.[50] Further analysis by coarse-grained molecular dynamics simulations show that the microscopic and macroscopic differences in sac structure are related to the mechanism of contact layer formation immediately after initial contact between the two solutions. In the case of spherical PA assemblies, PA diffuses into the HA compartment, the opposite of the direction of diffusion in traditional sacs.

We began by making sacs with **PA-1** and authentic **PA-2** without irradiation to confirm their structures. Sacs were made by injecting a drop of HA solution into a bath of PA. SEM images of the fixed and dehydrated sac samples (Figure 3) show that the structures of hierarchical HA membranes assembled with **PA-1** and **PA-2** are in agreement with previous reports. The three-zone morphology is clearly seen in the cross section of the HA/**PA-2** membranes (Figures 3B and S1), with the fibers perpendicular to the surface clearly visible (labeled zone 3). This organized structure is not observed in the HA/**PA-1** membrane (Figure 3A), where a thicker cross section with finger-like branches extending from the PA to the HA side exists. In this case, the structure does not display the characteristic order seen in the HA/**PA-2** sacs, indicating that a diffusion barrier has not formed. SAXS results (Figure 3D) reveal that the differences in membrane structure observed by SEM are also manifested in the nanoscale structure. The scattering pattern of a sac made with **PA-2** exhibits a broad peak (blue line in Figure 3D; q_{max} = 0.086 Å^{-1}), while the scattering pattern of a sac made with **PA-1** shows two Bragg peaks (red line in Figure 3D; $q_{max,1}$ = 0.068 Å^{-1}, $q_{max,2}$ = 0.123 Å^{-1}) indicative of a closely packed organization.

In order to examine our ability to attain dynamic control over the self-assembled membrane structure, we designed an experiment where the PA nanostructure would change from sphere to cylinder during the formation of the sac. For this experiment, we added a drop of HA solution to a solution of **PA-1** and allowed the sac to mature. The entire solution was then irradiated, inducing the transition to cylindrical PA nanostructures. We expected to observe a thick, dense cross section, consistent with sacs made from **PA-1**, combined with perpendicular fibers at the surface, consistent with sacs made from **PA-2**. The results of the experiment are shown in Figure 3C. SEM confirmed our expectations, revealing that the irradiated sac shows characteristics of membranes made from both **PA-1** and **PA-2**, namely, a thick cross-section and perpendicular fiber growth. This type of complex hierarchical structure has not been previously observed and demonstrates the power of light-driven changes in molecular structure to create new soft materials.

Based on the SEM and SAXS data of the irradiated sac, we propose the following mechanism of formation: The initial complexation between HA and the spherical micelles of **PA-1** forms an amorphous layer as PA diffuses into the HA droplet. Irradiation induces a conversion of the PA from spheres to cylinders, and we speculate that a diffusion barrier between HA and **PA-2** forms at the surface of the sac. The thick layer formed in the initial complexation does not appear to prevent

the formation of a diffusion barrier once cylinder-forming **PA-2** is generated by photolysis. The diffusion barrier is difficult to see in the SEM image, but the presence of perpendicular fibers in Figure 3C attest to its presence. Additionally, irradiation does not appear to affect the initial complexation region made from HA and **PA-1**. Once the diffusion barrier forms, perpendicular fibers composed of HA and **PA-2** are formed by reptation of HA through the HA/**PA-1** complexation region and the HA/**PA-2** diffusion barrier. This conclusion is supported by the presence of two Bragg peaks in the SAXS trace (purple line in Figure 3D), where q_{max} values are similar to those observed from sacs made with **PA-2**. Compared with the sac from **PA-2**, the peaks are less pronounced in the case of the irradiated sac, likely as a result of either overlapping between the two Bragg peaks and the broad peak or the smaller number of closely packed domains. Overall, the mechanism is consistent with a combination of the mechanisms for sac formation between HA and PA in either spherical or cylindrical assemblies.

We have employed here a photocleavable PA in the design of a hierarchically assembled structure. By triggering the photocleavage during the self-assembly process, a mixed HA-PA sac structure was attained. We propose that the exposure of the sac to UV light thus leads to a change in the direction of HA-PA diffusion during sac formation: PA diffuses into the HA compartment before irradiation, as has been previously shown for spherical PA assemblies;[50] after irradiation, the HA diffuses into the PA compartment, which is the common mode of sac formation for cylindrical PA assemblies.[3] To our knowledge, this work represents the first demonstration of dynamic, light-driven control of a hierarchical molecular self-assembly process. We expect that this strategy may be employable in the construction of other complex materials to create structures that cannot be made by one hierarchical self-assembly process alone.

■ ASSOCIATED CONTENT

ⓢ Supporting Information

Additional SEM images, SAXS traces and fitting parameters, synthetic details, and experimental procedures. This material is available free of charge via the Internet at http://pubs.acs.org.

■ AUTHOR INFORMATION

Corresponding Author

*E-mail: rbitton@exchange.bgu.ac.il. Tel.: +97286461499.

Present Address

‡Department of Chemistry, Virginia Tech, Blacksburg, VA 24061 (J.B.M.).

Notes

The authors declare no competing financial interest.

■ ACKNOWLEDGMENTS

■ REFERENCES

(1) Meyers, M. A.; Chen, P.-Y.; Lin, A. Y.-M.; Seki, Y. *Prog. Mater. Sci.* **2008**, *53*, 1−206.

(2) Fratzl, P.; Weinkamer, R. *Prog. Mater. Sci.* **2007**, *52*, 1263−1334.

(3) Capito, R. M.; Azevedo, H. S.; Velichko, Y. S.; Mata, A.; Stupp, S. I. *Science* **2008**, *319*, 1812−1816.

(4) Stupp, S. I.; Zha, R. H.; Palmer, L. C.; Cui, H. G.; Bitton, R. *Faraday Discuss.* **2013**, *166*, 9−30.

(5) Palmer, L. C.; Newcomb, C. J.; Kaltz, S. R.; Spoerke, E. D.; Stupp, S. I. *Chem. Rev.* **2008**, *108*, 4754−4783.

(6) Rybtchinski, B. *ACS Nano* **2011**, *5*, 6791−6818.

(7) Korevaar, P. A.; Schaefer, C.; de Greef, T. F. A.; Meijer, E. W. *J. Am. Chem. Soc.* **2012**, *134*, 13482−13491.

(8) Chow, L. W.; Bitton, R.; Webber, M. J.; Carvajal, D.; Shull, K. R.; Sharma, A. K.; Stupp, S. I. *Biomaterials* **2011**, *32*, 1574−1582.

(9) Carew, D. B.; Channon, K. J.; Manners, I.; Woolfson, D. N. *Soft Matter* **2011**, *7*, 3475−3481.

(10) Zha, R. H.; Sur, S.; Stupp, S. I. *Adv. Healthcare Mater.* **2013**, *2*, 126−133.

(11) Mendes, A. C.; Smith, K. H.; Tejeda-Montes, E.; Engel, E.; Reis, R. L.; Azevedo, H. S.; Mata, A. *Adv. Funct. Mater.* **2013**, *23*, 430−438.

(12) Hughes, M.; Xu, H.; Frederix, P. W. J. M.; Smith, A. M.; Hunt, N. T.; Tuttle, T.; Kinloch, I. A.; Ulijn, R. V. *Soft Matter* **2011**, *7*, 10032−10038.

(13) Wang, W.; Chau, Y. *Soft Matter* **2009**, *5*, 4893−4898.

(14) Ghosh, A.; Haverick, M.; Stump, K.; Yang, X. Y.; Tweedle, M. F.; Goldberger, J. E. *J. Am. Chem. Soc.* **2012**, *134*, 3647−3650.

(15) Veerman, C.; Rajagopal, K.; Palla, C. S.; Pochan, D. J.; Schneider, J. P.; Furst, E. M. *Macromolecules* **2006**, *39*, 6608−6614.

(16) Hamley, I. W.; Castelletto, V.; Moulton, C.; Myatt, D.; Siligardi, G.; Oliveira, C. L. P.; Pedersen, J. S.; Abutbul, I.; Danino, D. *Macromol. Biosci.* **2010**, *10*, 40−48.

(17) Bowerman, C. J.; Liyanage, W.; Federation, A. J.; Nilsson, B. L. *Biomacromolecules* **2011**, *12*, 2735−2745.

(18) Pochan, D. J.; Schneider, J. P.; Kretsinger, J.; Ozbas, B.; Rajagopal, K.; Haines, L. *J. Am. Chem. Soc.* **2003**, *125*, 11802−11803.

(19) Wright, E. R.; Conticello, V. P. *Adv. Drug Delivery Rev.* **2002**, *54*, 1057−1073.

(20) Xu, C. Y.; Breedveld, V.; Kopecek, J. *Biomacromolecules* **2005**, *6*, 1739−1749.

(21) Besenius, P.; Portale, G.; Bomans, P. H. H.; Janssen, H. M.; Palmans, A. R. A.; Meijer, E. W. *Proc. Natl. Acad. Sci. U.S.A.* **2010**, *107*, 17888−17893.

(22) Sur, S.; Matson, J. B.; Webber, M. J.; Newcomb, C. J.; Stupp, S. I. *ACS Nano* **2012**, *6*, 10776−10785.

(23) Muraoka, T.; Cui, H.; Stupp, S. I. *J. Am. Chem. Soc.* **2008**, *130*, 2946−2947.

(24) Muraoka, T.; Koh, C.-Y.; Cui, H.; Stupp, S. I. *Angew. Chem., Int. Ed.* **2009**, *48*, 5946−5949.

(25) Haines, L. A.; Rajagopal, K.; Ozbas, B.; Salick, D. A.; Pochan, D. J.; Schneider, J. P. *J. Am. Chem. Soc.* **2005**, *127*, 17025−17029.

(26) Aikawa, S.; Shrestha, R. G.; Ohmori, T.; Fukukita, Y.; Tezuka, Y.; Endo, T.; Torigoe, K.; Tsuchiya, K.; Sakamoto, K.; Sakai, K.; Abe, M.; Sakai, H. *Langmuir* **2013**, *29*, 5668−5676.

(27) Ketner, A. M.; Kumar, R.; Davies, T. S.; Elder, P. W.; Raghavan, S. R. *J. Am. Chem. Soc.* **2007**, *129*, 1553−1559.

(28) Oh, H.; Ketner, A. M.; Heymann, R.; Kesselman, E.; Danino, D.; Falvey, D. E.; Raghavan, S. R. *Soft Matter* **2013**, *9*, 5025−5033.

(29) Velichko, Y. S.; Mantei, J. R.; Bitton, R.; Carvajal, D.; Shull, K. R.; Stupp, S. I. *Adv. Funct. Mater.* **2012**, *22*, 369−377.

(30) Webber, M. J.; Newcomb, C. J.; Bitton, R.; Stupp, S. I. *Soft Matter* **2011**, *7*, 9665−9672.

(31) Gao, Y.; Yang, Z. M.; Kuang, Y.; Ma, M. L.; Li, J. Y.; Zhao, F.; Xu, B. *Biopolymers* **2010**, *94*, 19−31.

(32) Chau, Y.; Luo, Y.; Cheung, A. C. Y.; Nagai, Y.; Zhang, S.; Kobler, J. B.; Zeitels, S. M.; Langer, R. *Biomaterials* **2008**, *29*, 1713−1719.

(33) Galler, K. M.; Aulisa, L.; Regan, K. R.; D'Souza, R. N.; Hartgerink, J. D. *J. Am. Chem. Soc.* **2010**, *132*, 3217−3223.

(34) Lock, L. L.; Cheetham, A. G.; Zhang, P.; Cui, H. *ACS Nano* **2013**, *7*, 4924−4932.

(35) Matson, J. B.; Zha, R. H.; Stupp, S. I. *Curr. Opin. Solid State Mater. Sci.* **2011**, *15*, 225−235.

(36) Silva, G. A.; Czeisler, C.; Niece, K. L.; Beniash, E.; Harrington, D. A.; Kessler, J. A.; Stupp, S. I. *Science* **2004**, *303*, 1352−1355.

(37) Mata, A.; Geng, Y. B.; Henrikson, K. J.; Aparicio, C.; Stock, S. R.; Satcher, R. L.; Stupp, S. I. *Biomaterials* **2010**, *31*, 6004−6012.

(38) Shah, R. N.; Shah, N. A.; Lim, M. M. D.; Hsieh, C.; Nuber, G.; Stupp, S. I. *Proc. Natl. Acad. Sci. U.S.A.* **2010**, *107*, 3293−3298.

(39) Huang, Z.; Newcomb, C. J.; Bringas, P.; Stupp, S. I.; Snead, M. L. *Biomaterials* **2010**, *31*, 9202−9211.

(40) Tysseling-Mattiace, V. M.; Sahni, V.; Niece, K. L.; Birch, D.; Czeisler, C.; Fehlings, M. G.; Stupp, S. I.; Kessler, J. A. *J. Neurosci.* **2008**, *28*, 3814−3823.

(41) Yu, Y. C.; Berndt, P.; Tirrell, M.; Fields, G. B. *J. Am. Chem. Soc.* **1996**, *118*, 12515−12520.

(42) Hartgerink, J. D.; Beniash, E.; Stupp, S. I. *Science* **2001**, *294*, 1684−1688.

(43) Cui, H.; Webber, M. J.; Stupp, S. I. *Biopolymers* **2010**, *94*, 1−18.

(44) Cui, H.; Muraoka, T.; Cheetham, A. G.; Stupp, S. I. *Nano Lett.* **2009**, *9*, 945−951.

(45) Velichko, Y. S.; Stupp, S. I.; de la Cruz, M. O. *J. Phys. Chem. B* **2008**, *112*, 2326−2334.

(46) Lee, O. S.; Stupp, S. I.; Schatz, G. C. *J. Am. Chem. Soc.* **2011**, *133*, 3677−3683.

(47) Greenfield, M. A.; Hoffman, J. R.; de la Cruz, M. O.; Stupp, S. I. *Langmuir* **2010**, *26*, 3641−3647.

(48) Paramonov, S. E.; Jun, H. W.; Hartgerink, J. D. *J. Am. Chem. Soc.* **2006**, *128*, 7291−7298.

(49) Goldberger, J. E.; Berns, E. J.; Bitton, R.; Newcomb, C. J.; Stupp, S. I. *Angew. Chem., Int. Ed.* **2011**, *50*, 6292−6295.

(50) Bitton, R.; Chow, L. W.; Zha, R. H.; Velichko, Y. S.; Pashuck, E. T.; Stupp, S. I. *Small* **2014**, *10*, 500−505.

(51) Carvajal, D.; Bitton, R.; Mantei, J. R.; Velichko, Y. S.; Stupp, S. I.; Shull, K. R. *Soft Matter* **2010**, *6*, 1816−1823.